Segmental Uveoscleral Outflow and its Relationship With Trabecular Outflow in Monkey Eyes

Hoi-Lam Li,[1] Su Yu,[1,3] Shan Fan,[4] Carol B. Toris,[4,5] and Haiyan Gong[1,2]

[1]Department of Ophthalmology, Boston University Chobanian & Avedisian School of Medicine, Boston, Massachusetts, United States
[2]Department of Anatomy and Neurobiology, Boston University Chobanian & Avedisian School of Medicine, Boston, Massachusetts, United States
[3]Massachusetts Eye Research and Surgery Institution, Boston, Massachusetts, United States
[4]Department of Ophthalmology and Visual Science, University of Nebraska Medical Center, Omaha, Nebraska, United States
[5]Department of Ophthalmology and Visual Sciences, The Ohio State University, Columbus, Ohio, United States

Correspondence: Haiyan Gong, Department of Ophthalmology, Boston University Chobanian & Avedisian School of Medicine, 72 East Concord Street, Room L-905, Boston, MA 02118, USA; hgong@bu.edu.

Received: January 28, 2025
Accepted: April 4, 2025
Published: April 28, 2025

Citation: Li HL, Yu S, Fan S, Toris CB, Gong H. Segmental uveoscleral outflow and its relationship with trabecular outflow in monkey eyes. *Invest Ophthalmol Vis Sci.* 2025;66(4):78. https://doi.org/10.1167/iovs.66.4.78

Purpose. Segmental trabecular outflow has been observed in various species, and we recently reported segmental uveoscleral outflow in mouse eyes. However, whether this pattern exists in other species remains unclear. This study aimed to investigate segmental uveoscleral outflow and its correlation with trabecular outflow in monkey eyes.

Methods. Five healthy eyes of aged cynomolgus macaques were examined. After anesthesia, a fixed volume of tracer was injected into the anterior chamber and allowed to diffuse for 45 minutes before fixation. The eyes were dissected into 12 radial segments, and images were captured using a confocal microscope. Segments were randomly selected for histological study. Tracer intensity and stromal thickness were measured.

Results. Four distinct tracer patterns were observed: (1) low flow in both pathways, (2) high flow (HF) in both, (3) HF in trabecular outflow, and (4) HF in uveoscleral outflow. As trabecular outflow contributed 75% of the total outflow, the "HF in uveoscleral outflow" pattern was the least frequent. Segmental flow patterns were observed in both outflow pathways, including components along the uveoscleral outflow pathway: supraciliary and suprachoroidal spaces, spaces between muscle bundles, and ciliary stroma. A positive correlation was found between tracer intensity along the uveoscleral outflow pathway and stromal thickness.

Conclusions. Uveoscleral outflow is segmental and uncorrelated with trabecular outflow in monkey eyes. It primarily occurs in the ciliary stroma, where it positively correlates with stromal thickness. Future studies in human eyes may inform the optimal placement of drainage devices and drug delivery systems targeting the uveoscleral outflow pathway.

Keywords: aqueous humor dynamic, uveoscleral outflow, trabecular outflow, monkey, segmental outflow

Aqueous humor (AH) exits the eye through two primary outflow pathways: trabecular (conventional) and uveoscleral (unconventional) outflow pathways.[1,2] In the trabecular outflow pathway, AH traverses the trabecular meshwork (TM) followed by Schlemm's canal (SC), collector channels, aqueous veins, and episcleral veins. Conversely, the uveoscleral outflow pathway presents a more complex route, with AH dispersing into various compartments, including the supraciliary and suprachoroidal spaces (SCS), interstitial spaces between ciliary muscle bundles (IM), and the stroma of the ciliary process.[3,4] Eventually, AH exits the eye across the sclera through the vortex veins[5,6] or via the orbital vasculature.[7,8]

Elevated intraocular pressure (IOP), resulting from increased resistance in the outflow pathways, is the primary risk factor for primary open-angle glaucoma (POAG). Lowering IOP through different pharmaceutical agents, laser therapy, or surgical intervention targeting the outflow pathways[9–14] is the current clinical intervention to delay the progression of visual field defect.[15–17] Segmental trabecular outflow has been reported in various species, including mice,[18–21] porcine,[22] bovine,[23] monkeys,[24–26] and humans,[27–30] using tracer injections and fluorescein aqueous angiography. Studies have also identified biomechanical and morphological differences between high-flow (HF) and low-flow (LF) regions in glaucomatous[31] or laser-induced ocular hypertensive[25,26] eyes. Remarkably, studies have shown that different locations of trabecular bypass surgery[13] and 180 degrees selective laser trabeculoplasty[14] can result in significantly different IOP reductions. Given the critical role of both outflow pathways in IOP regulation, understanding their flow patterns and interactions is essential for developing targeted and effective therapies. Our previous work demonstrated that uveoscleral outflow is segmental in mouse eyes and uncorrelated with trabecular outflow.[20] Yet, the flow pattern of uveoscleral outflow in other species

is unknown. Building upon these insights, we hypothesize that both uveoscleral and trabecular outflow are segmental and uncorrelated. Furthermore, we propose that a segmental pattern is also observed in the different components along the uveoscleral outflow pathway. This study aims to elucidate the flow pattern of uveoscleral outflow and its relationship with trabecular outflow in healthy monkey eyes.

Materials and Methods

All experimental procedures were approved by the Institutional Animal Care and Use Committee of the University of Nebraska Medical Center and Covance Laboratories, Inc. (Madison, WI, USA), in compliance with the ARVO Statement for the Use of Animals in Ophthalmic and Vision Research. Five female cynomolgus macaques, aged 20 ± 1 years, were used in this study. These monkeys had participated in prior minimally invasive experiments for 10 to 15 years at the University of Nebraska Medical Center. The final minimally invasive procedure involved injecting 100 µL of either hyaluronic acid-based hydrogel or saline solution into the SCS region at the 7 to 8 o'clock position. There was at least a 2-month recovery period between studies, and the IOP returned to baseline levels before the current study. No significant difference in IOP was found between hydrogel- and saline-injected eyes ($P > 0.05$, two-tailed Mann-Whitney U test). The endpoint IOP was 19.7 ± 1.9 millimeters of mercury (mm Hg), and no abnormalities were observed in the eyes.

Tracer Injection

The monkeys were anesthetized initially with an intramuscular injection of ketamine (10 mg/kg body weight) and maintained anesthetized with 2.5% isoflurane. A fixed volume (50 µL) of 200 nm FluoSpheres (Ex/Em: 505/515; Invitrogen, Carlsbad, CA, USA), diluted 1:50 in Dulbecco's phosphate-buffered saline solution (v/v), was injected gradually into the anterior chamber. The tracers were allowed to diffuse and reach the outflow systems for 45 minutes. Subsequently, the eyes were fixed with 4% paraformaldehyde (PFA) in situ for 30 minutes. Following euthanasia, the 12 o'clock position was marked on the globes. The eyes were enucleated and fixed in 4% PFA at 4°C for 48 hours. The fixed eyes were transferred to a saline solution and shipped from the University of Nebraska Medical Center to Boston University for imaging analysis.

Confocal Microscopy

All procedures for confocal imaging followed a previously published protocol.[20] The eyes were dissected into 12 equal radial segments. After nuclear counterstaining with DAPI (Vector Laboratories, Inc., Newark, CA, USA), each segment was placed on a glass-bottom plate with its cross-section facing downward. Cross-sections from both sides of the radial segments were imaged using a confocal microscope (Zeiss LSM 700 confocal microscope; Carl Zeiss, White Plains, NY, USA). The confocal microscope is an inverted system with the objective lenses located beneath the stage, and all tracer signals were captured via z-stack imaging. An objective with 20× magnification and z-stack images with a step size of 1.5 µm, using the same setting of gain, digital offset, and pinhole size, were used for the imaging. The excitation wavelengths for the nucleus (blue) and tracer (green) were 405 nm (channel 0) and 488 nm (channel 1), respectively. No signal was observed in the control eyes with no tracer injection.

Analysis of Tracer Intensity in the Confocal Images

The right eyes with tracer were used for analysis. The superior and nasal sides were designated as 12 o'clock and 3 o'clock, respectively, with the remaining positions assigned as follows: 2 to 4 o'clock for nasal (N), 5 to 7 o'clock for inferior (I), 8 to 10 o'clock for temporal (T), and 11 to 1 o'clock for superior (S). Before analysis, two-dimensional images for both nucleus and tracer channels were generated from the stack images in each location using the Z Project function in ImageJ software, with maximum intensity projection as the method. Tracer intensity ranged from 0 (the darkest) to 255 (the brightest). The signal under 13 was set as the background, determined by control images collected from the non-tracer-injected eyes. In other words, all signals with intensity below 13 were removed. In pilot studies, we confirmed the structures with phase-contrast images using a confocal microscope and semi-thin (approximately 2 µm) section images using a light microscope (Fig. 1A). A line was drawn from the root of the iris to the scleral spur (SS) and along the SCS (see Fig. 1). Any tracer signal in the area above this line was considered a tracer in the trabecular outflow pathway, and the sum of tracer intensity in this area represented the total intensity in the trabecular outflow pathway. Signals in the area below the line were considered a tracer in the uveoscleral outflow pathway. Tracer intensity in the uveoscleral outflow pathway was the sum of total intensity in the SCS, stroma, and IM (see Fig. 1B). Using ImageJ software, two independent investigators performed all the image analyses twice, with less than 10% differences among readings. The total tracer intensity (the sum of all pixel values) of the individual eye was the sum of the tracer intensity along uveoscleral and trabecular outflow pathways on both sides of the 12 equal radial segments of each eye. The tracer intensity at different locations was normalized by dividing the total tracer intensity of each location by the total tracer intensity of the individual eye and then multiplying by 100 to express the results as percentages. Thus, the normalized tracer intensity at each clock-hour location represented the percentage of the total intensity at each clock-hour location within the uveoscleral or trabecular outflow pathway or within the SCS, IM, or ciliary stroma, divided by the total tracer intensity of the individual eye. Similarly, the normalized tracer intensity at different quadrants was calculated as the percentage of the sum of the total intensity at the clock-hour locations within each quadrant divided by the total tracer intensity of the individual eye.

Histology

The confocal images with clear stroma structures identified by nucleus staining were used to measure the thickness of the stroma. The boundary of the ciliary stroma was marked in ImageJ. Then, the thickness of the stroma was measured at three different positions of the stroma: near the iris (beginning), in the middle, and near the ciliary process (end), automatically by using Python code

Investigative Ophthalmology & Visual Science

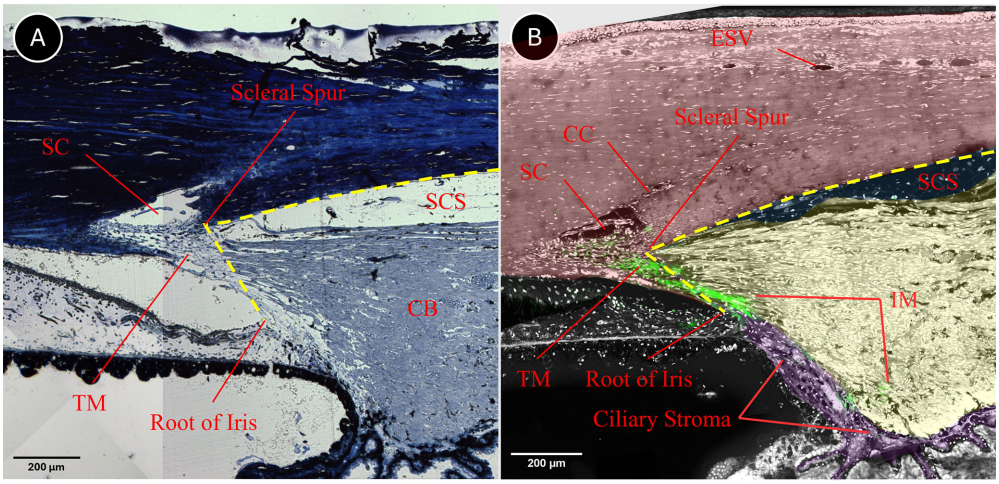

Figure 1. Methods for segmenting tracer intensity in the trabecular and uveoscleral outflow pathways. The representative anterior structure of a normal monkey eye was captured using (**A**) a light microscope after staining with 1% toluidine blue and (**B**) a confocal microscope after DAPI staining. In panel **B**, the nuclei appears *white*, and the tracer appears *green*. A *yellow dotted line* is drawn from the root of the iris to the scleral spur, following the supraciliary and suprachoroidal spaces (SCS). The tracer in the area above the *yellow dotted line* (*shaded in red*; Supplementary Figs. S1D–S1F) corresponds to the trabecular outflow pathway, whereas the tracer in the area below the *yellow dotted line* corresponds to the uveoscleral outflow pathway. The tracer intensity in uveoscleral outflow is the sum of tracer intensity in the SCS region (*blue-shaded*; Supplementary Figs. S1G–S1I), the interstitial spaces between the ciliary muscle bundles (IM) region (*yellow-shaded*; Supplementary Figs. S1J–S1L), and the ciliary stroma (*purple-shaded*, Supplementary Figs. S1M–S1O). ESV, episcleral vein; CC, collector channel; SC, Schlemm's canal; TM, trabecular meshwork; CB, ciliary body.

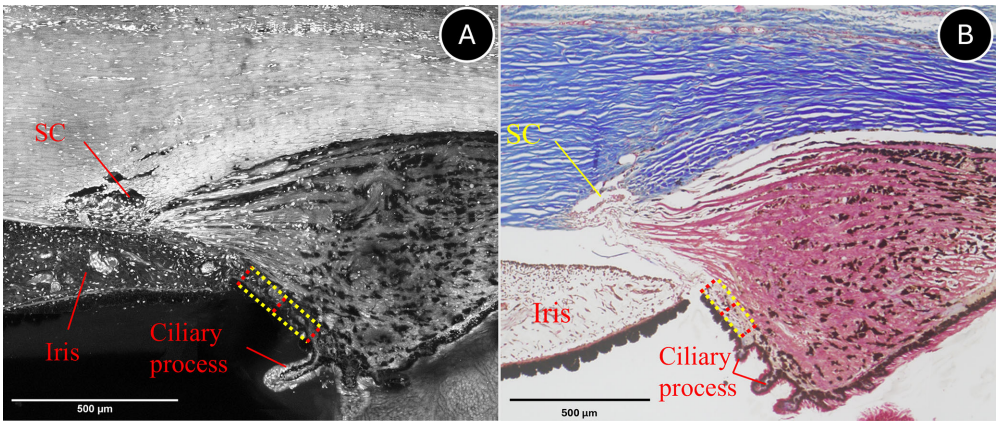

Figure 2. Methods for measuring stromal thickness. The representative anterior structure of a healthy monkey eye was captured using (**A**) a confocal microscope after DAPI staining and (**B**) a light microscope after Masson's trichrome staining. In panel **A**, the nuclei appear *white*. In panel **B**, collagen fibers stain *blue*, and ciliary muscle fibers stain *red*. The *yellow dotted line* marks the stromal boundary between the iris and the first ciliary process using ImageJ. Stromal thickness (*red dotted line*) was measured automatically at the beginning (near the iris), middle, and end (near the ciliary process) by the Python code in PyCharm software. SC, Schlemm's canal.

in PyCharm software (version 2023.2.7; Community Edition; JetBrains). The average of the thickness measured at the three positions was calculated for analysis (Fig. 2A). Segments from four to six locations with different intensities along uveoscleral outflow pathways were randomly selected from each eye. The segments were cleared with xylene after dehydration with a graded ethanol series (70%–100%). The cleared segments were then embedded in paraffin and sectioned to 8 to 10 µm thickness. The sections were rehydrated through a reverse ethanol series and stained using Masson's trichrome. Finally, the sections were mounted with Permount Mounting Medium and imaged by a light microscope (Olympus FSX100). Based on the histological structure, stromal thickness was measured following the same protocol used for confocal images (Fig. 2B).

Statistical Analysis

All statistical analyses were performed using GraphPad Prism (version 9.5.1; GraphPad Software, San Diego, CA, USA). Twenty-four images were analyzed for each eye, and the mean tracer intensity in both trabecular and uveoscleral outflow pathways was calculated for each eye. Regions of LF and HF were defined as tracer intensities below or above the individual mean for each eye, respectively. The frequency of

Investigative Ophthalmology & Visual Science

different outflow patterns (i.e. the percentage of each pattern in each eye relative to the total 24 images per eye) was compared using the Friedman test, followed by an uncorrected Dunn's test as a post hoc analysis. Two-way repeated measures ANOVA, followed by Uncorrected Fisher's least significant difference (LSD) post hoc test, were used to compare the normalized tracer intensity in the outflow pathways at different locations in both trabecular and uveoscleral outflow. Meanwhile, one-way repeated measures ANOVA was used to compare the normalized tracer intensity in the IM, SCS, and ciliary stroma. A Spearman correlation test was performed to investigate various correlations, including the correlation between the normalized tracer intensity in the trabecular and uveoscleral outflow pathways, between the normalized tracer intensity in SCS/IM/ciliary stroma and along the uveoscleral outflow pathways, as well as between the tracer intensity along the uveoscleral outflow pathway and stromal thickness. Outliers were identified using the Robust Regression and Outlier Removal (ROUT) test with a false discovery rate (Q) value of 1%. A P value of < 0.05 was considered statistically significant ($^{*}P < 0.05$; $^{**}P < 0.01$, $^{***}P < 0.001$, $^{****}P < 0.0001$).

Results

Segmental Trabecular and Uveoscleral Outflow in Monkey Eyes

Four different patterns of the tracer distribution were observed. They were (1) LF in both outflow pathways (Fig. 3A), (2) HF in both outflow pathways (Fig. 3B), (3) HF predominantly in the trabecular outflow pathway (Fig. 3C), and (4) HF predominantly in the uveoscleral outflow pathway (Fig. 3D). The frequency of the "HF predominantly in the trabecular outflow pathway" pattern was the highest. This was significantly higher than the "LF in both outflow pathways" by 27 ± 17% ($P < 0.05$) and the "HF predominantly in the uveoscleral outflow pathway" by 56 ± 11% ($P < 0.01$; Fig. 4). After analyzing all the tracer intensities, the results showed that both trabecular and uveoscleral outflow patterns were segmental and uncorrelated ($P > 0.05$). The normalized tracer intensity in uveoscleral outflow was the highest at the 11 o'clock location and lowest at the 3 o'clock location, with a marginal trend toward significance ($P = 0.0579$) between these 2 clock hour locations. In the trabecular outflow pathway, the normalized tracer inten-

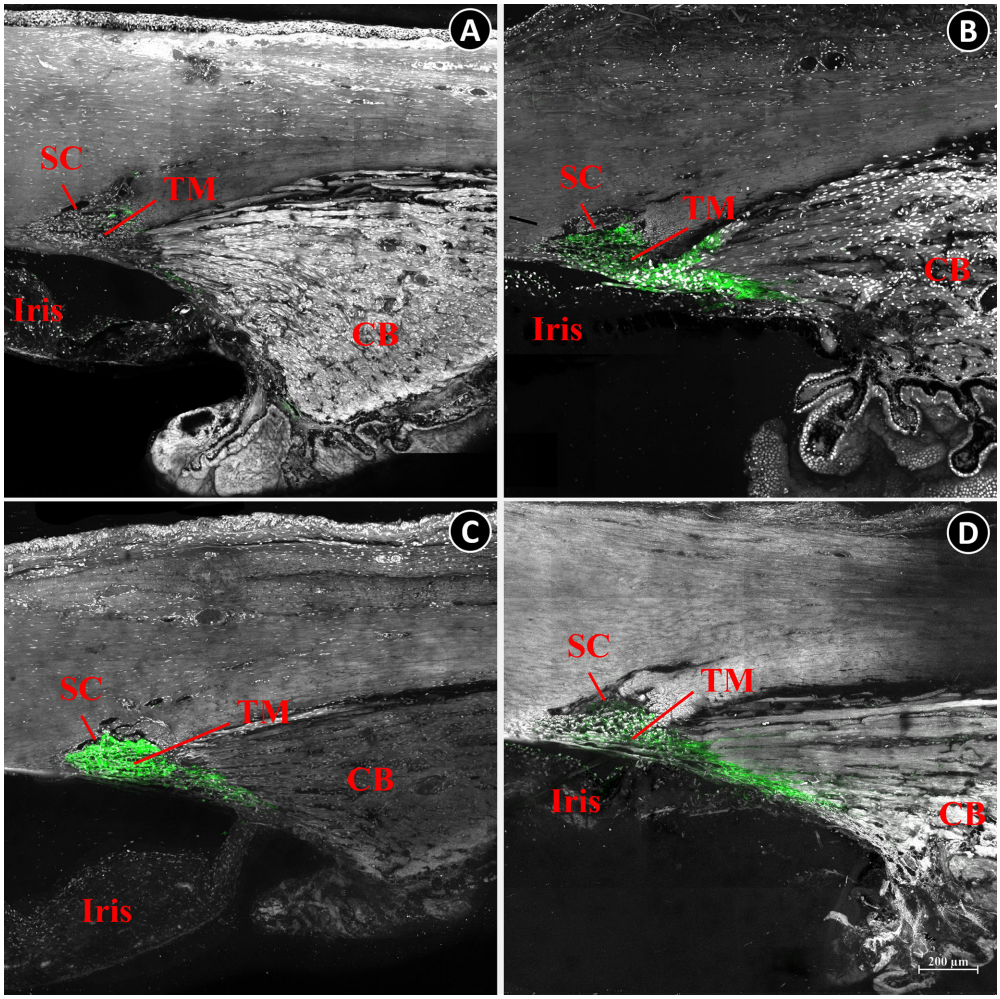

Figure 3. Four outflow patterns. Representative images showing the following tracer distribution patterns: (**A**) low tracer intensity in both outflow pathways; (**B**) high tracer intensity in both outflow pathways; (**C**) high tracer intensity predominantly in the trabecular outflow pathway; and (**D**) high tracer intensity predominantly in the uveoscleral outflow pathway. SC, Schlemm's canal; TM, trabecular meshwork; CB, ciliary body.

Investigative Ophthalmology & Visual Science

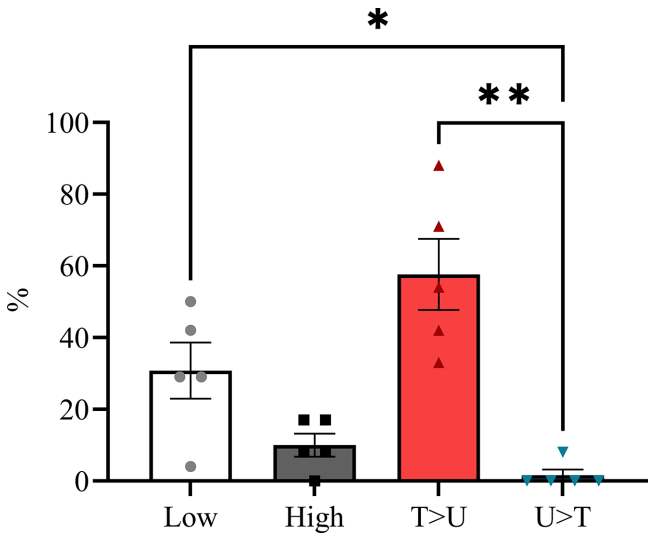

Figure 4. Distribution of four outflow patterns. After comparing with the mean normalized tracer intensity for both the trabecular and uveoscleral outflow pathways in each eye, the mean percentage of each outflow pattern relative to the total images per eye is presented: (1) LF in both outflows (low); (2) HF in both outflows (high); (3) HF in trabecular outflow pathway only (T > U); and (4) HF in uveoscleral outflow only (U > T).

sity was the highest at the 2 o'clock location and lowest at the 5 o'clock location, with a significant difference of 4.4 ± 3.5% ($P < 0.01$). The normalized tracer intensity was significantly higher in the trabecular outflow pathway than in the uveoscleral outflow pathway at the 1, 2, 3, 4, 8, 9, and 10 o'clock positions by 5% to 7% (Fig. 5A). A high-flow region was identified in the superior quadrant of the uveoscleral outflow pathway and in the nasal quadrant of the trabecular outflow pathway. The LF regions of uveoscleral and trabecular outflow were mainly located in the nasal and inferior quadrants, respectively. Similar to the comparison across clock hours, a significant difference was observed in the trabecular outflow pathway between the HF (nasal) and LF (inferior) regions ($P < 0.05$), but no significant difference was found in the uveoscleral outflow pathway. The normalized tracer intensity was significantly higher in the trabecular outflow pathway than in the uveoscleral outflow pathway at all quadrants except the inferior quadrant by a maximum of 17.2 ± 5.3% (Fig. 5B). Therefore, the overall normalized tracer intensity was also significantly higher in the trabecular outflow than in the uveoscleral outflow ($P < 0.05$) in a ratio of 3:1.

Segmental Outflow Pattern in Different Regions Along the Uveoscleral Outflow Pathway

Segmental normalized tracer distribution was also observed in the three components along the uveoscleral outflow pathways: SCS (Fig. 6A), IM (Fig. 6B), and ciliary stroma (Fig. 6C). The high tracer intensity regions were mainly located at the 6 and 11 o'clock position. Whereas the low tracer intensity regions were mainly located between the 1 and 3 o'clock positions. The maximum significant difference was found between the 2 and 6 o'clock positions in SCS (0.06 ± 0.02%, $P < 0.05$), the 8 and 9 o'clock positions in IM (0.38 ± 0.14%, $P < 0.05$), and the 9 and 11 o'clock positions in the ciliary stroma (1.45 ± 0.48%, $P < 0.05$). Combining all the tracers observed around the eyes (Fig. 6D), the normalized tracer intensity was the highest in the ciliary stroma, significantly greater than that in the IM by 7.2 ± 2.3% ($P < 0.05$) and in the SCS by 15.7 ± 3.8% ($P < 0.05$). Besides, the normalized tracer intensity in IM and stroma were significantly positively correlated with that in the uveoscleral outflow pathway ($P < 0.05$).

Correlation Between the Thickness of Stroma and Tracer Intensity Along Uveoscleral Outflow

Our results showed that higher tracer intensity along the uveoscleral outflow pathway (Fig. 7A) was associated with thicker stroma (Fig. 7B), whereas lower tracer intensity (Fig. 7C) was observed when the stroma thickness was smaller (Fig. 7D). After reviewing all the confocal images, 98 images were selected for measuring the thickness of the stroma (at least 17 images were measured for each eye). A positive correlation was found between the thickness of the stroma and the tracer intensity along the uveoscleral outflow pathway ($P < 0.0001$; Fig. 7E). This correlation was also observed in histological sections after Masson's trichrome staining, where the tracer intensity and stromal thickness were positively correlated ($P < 0.05$; Fig. 7F).

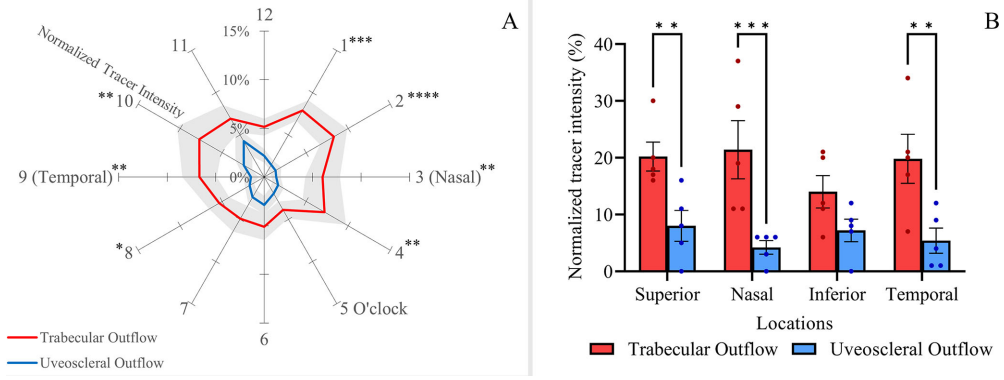

Figure 5. Tracer distribution in both uveoscleral and trabecular outflows around the eye. (**A**) *Solid red* and *blue lines* represent the mean normalized tracer intensity in the trabecular and uveoscleral outflow pathways at different clock hour locations. The *gray-shaded* zone represents the standard error of the mean (SEM). (**B**) The *red* and *blue bars* represent the mean normalized tracer intensity in the trabecular and uveoscleral outflow pathways in the different quadrants (*$P < 0.05$, **$P < 0.01$, ***$P < 0.001$, ****$P < 0.0001$).

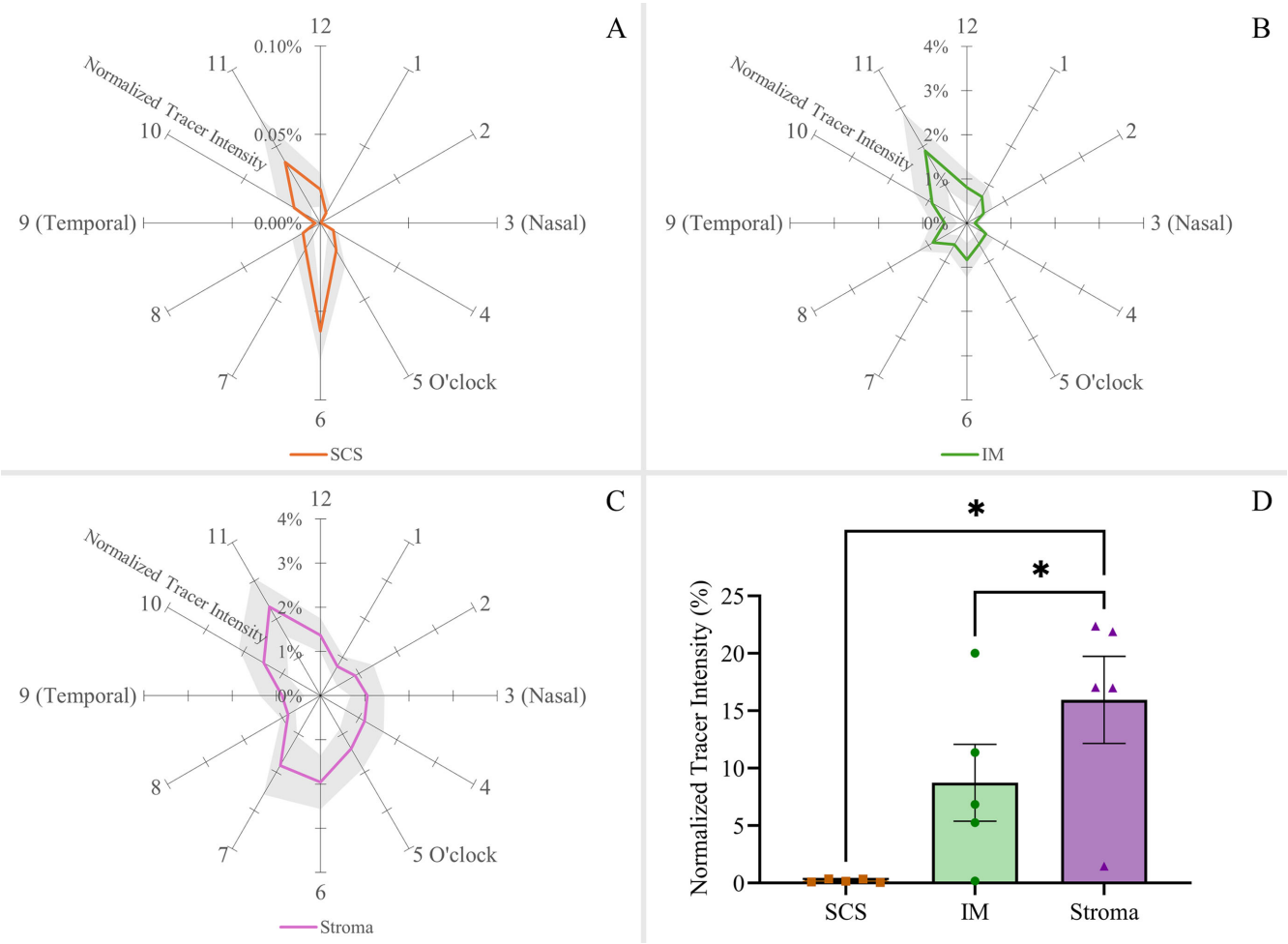

Figure 6. Segmental outflow pattern in different regions along the uveoscleral outflow pathway. Normalized tracer intensity in (**A**) supraciliary and suprachoroidal spaces (SCS), (**B**) interstitial spaces between muscle bundles (IM), and (**C**) ciliary stroma. (**D**) Total normalized tracer intensity in these three regions (*$P < 0.05$).

Discussion

This study investigates the flow patterns in both outflow pathways using the analysis method described in our previous study.[20] The tracer intensity at different clock hour locations was compared quantitatively between the two pathways. Our results showed that both uveoscleral and trabecular outflows are segmental and uncorrelated in healthy monkey eyes, which is consistent with findings in healthy mouse eyes.[20] The LF and HF regions of trabecular outflow were primarily located in the inferior region and in the superior and nasal regions, respectively, similar to the trend observed in the mouse eyes[20] and the TM side of human eyes.[28,29] Our results indicated that the LF and HF regions of the uveoscleral pathway were primarily located in the nasal and temporal regions and in the superior and inferior regions, respectively, differing from the pattern observed in mouse eyes.[20] However, similar to mouse eyes, four distinct flow patterns were observed in monkey eyes when reviewing all locations around the eye: (1) LF in both outflow pathways, (2) HF in both outflow pathways, (3) HF predominantly in the trabecular outflow pathway, and (4) HF predominantly in the uveoscleral outflow pathway. Notably, because trabecular outflow contributed more overall than uveoscleral outflow, the frequency of the "HF predominantly in the uveoscleral outflow pathway" pattern was limited compared to the mouse eyes.[20]

Focusing on the uveoscleral outflow pathways, the segmental pattern was reported in both CB and SCS in healthy mouse eyes. In contrast to mouse eyes, monkey eyes have a more distinct structure of the TM, scleral spur, ciliary muscles, and ciliary stroma. Therefore, we performed a more detailed analysis of uveoscleral outflow. Our results revealed a segmental flow pattern in the SCS, IM, and the ciliary stroma in healthy monkey eyes. Thus, our results suggest that uveoscleral outflow is segmental, involving the SCS, IM, and ciliary stroma, and it is uncorrelated with the trabecular outflow pattern in healthy monkey eyes.

Forty-five minutes after tracer injection, our results revealed that along the uveoscleral outflow pathways, most of the tracer was located in the ciliary stroma, with less tracer observed along the SCS, similar to findings in mouse eyes.[20] The normalized tracer intensity in the ciliary stroma was positively correlated with uveoscleral outflow, suggesting that the ciliary stroma has lower resistance compared with other structures. To further investigate this, we measured stromal thickness using two different sets of images with distinct processing and staining methods in order to rein-

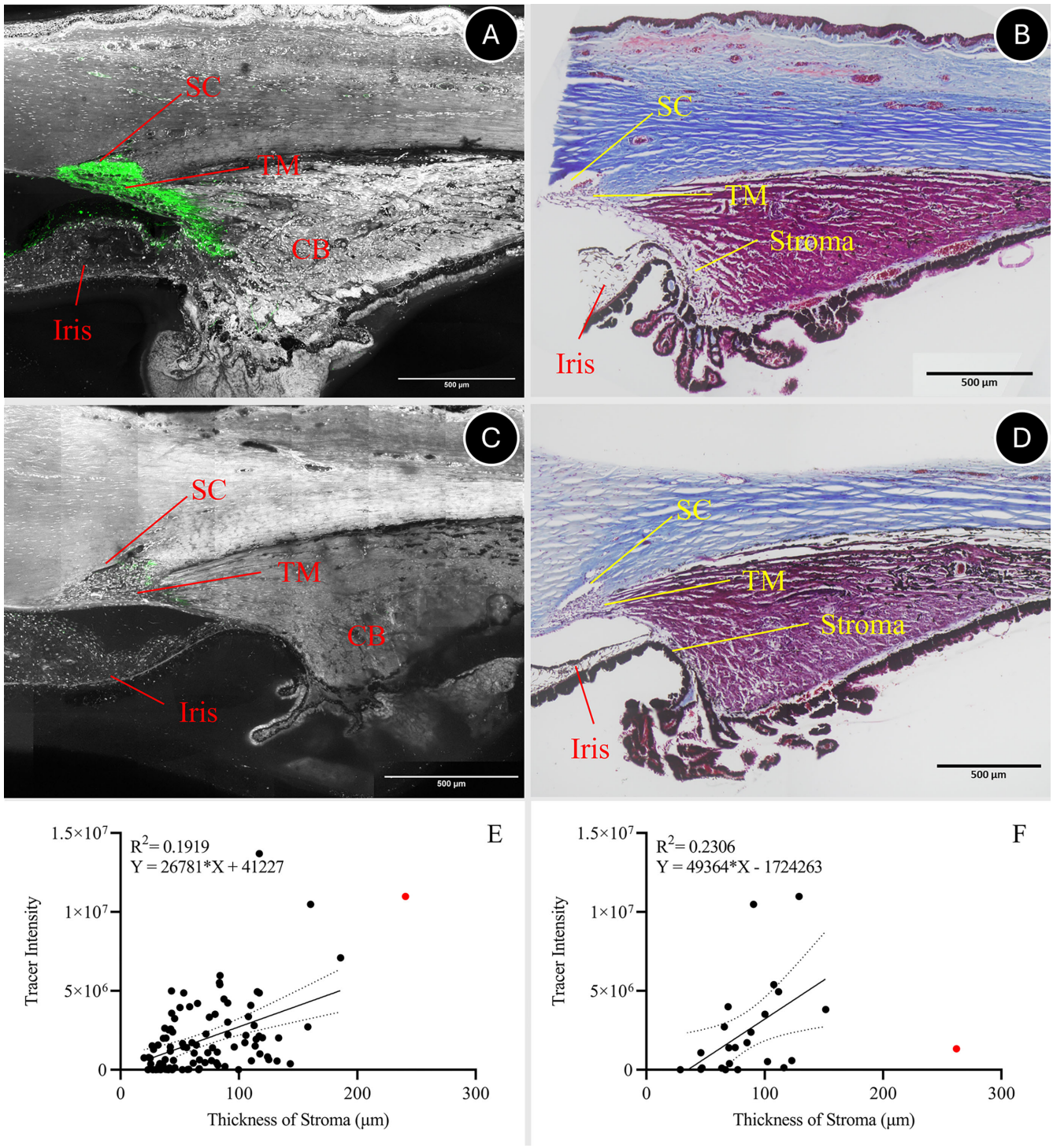

Figure 7. Correlation between uveoscleral outflow tracer intensity and stromal thickness. Representative image showing (**A**) high tracer intensity in the uveoscleral outflow pathway in confocal images and (**B**) greater stromal thickness in the same location observed in Masson's trichrome-stained sections; (**C**) low tracer intensity in the uveoscleral outflow pathway in confocal images; and (**D**) smaller stromal thickness in the corresponding location. A positive correlation was observed between tracer intensity and stromal thickness, as measured (**E**) in confocal images after DAPI staining and (**F**) in Masson's trichrome-stained sections. The outliers are labeled as the *red dots* in panels **E** and **F**. SC, Schlemm's canal; TM, trabecular meshwork; CB, ciliary body.

force the reliability and reproducibility of our findings. Both methods showed a positive correlation between stromal thickness and tracer intensity in the uveoscleral outflow. These findings support the hypothesis that as stromal spaces increase, resistance decreases, allowing more tracers to flow into the ciliary stroma. However, these results were only observed after 45 minutes of tracer injection, which may not have allowed sufficient time for the tracers to reach other

structures. Future studies with different waiting times would help clarify the entire process of uveoscleral outflow.

In addition to identifying the segmental outflow pattern and correlations in both outflow pathways at different positions, our analysis indicated that uveoscleral outflow constitutes approximately 25% of the total outflow in monkey eyes. This finding is comparable to previous studies in monkey eyes (20%–35%), which estimated the uveoscleral outflow by directly measuring the radioactive material concentration along the uveoscleral outflow pathway.[32,33] However, direct measurement of uveoscleral outflow has limitations, including the effect of perfusion/waiting duration and the size and surface properties of the tracer/perfused materials,[6,34,35] which may lead to errors, such as overestimation due to tracer retention in the tissue. Apart from the direct measurement of uveoscleral outflow, the uveoscleral outflow can be calculated by the indirect estimation using the modified Goldmann equation,[3,34] which may lead to varying estimations. For example, the uveoscleral outflow can vary from 0.14 ± 1.20 µL/min (measured by indirect estimation, 9% of the total outflow) to 1.05 ± 0.58 µL/min (measured by direct measurement, 70% of the total outflow) in the cynomolgus monkey.[36] Like direct measurements, indirect measurements also have limitations, as small errors in each factor of the equation (U = Qin – C (IOP - Pe); where U is the unconventional outflow, Qin is the AH inflow, C is the conventional outflow facility, and Pe is the episcleral venous pressure) can result in relatively large errors in outflow rate estimation. Although there is no ideal protocol to measure uveoscleral outflow, the current method allows us to quantify both outflow pathways around the eyes. Further studies with various post-injection times and tracer sizes are warranted to optimize the trabecular and uveoscleral outflow measurement protocols.

Given that measurement methods may vary, we compared the current results with our previous study in mouse eyes using the same analysis method. We found that the uveoscleral outflow contributes about 45% of the total outflow in mouse eyes[20] but only 25% in monkey eyes. This suggests that trabecular outflow plays a more significant role in the overall outflow dynamics in aged monkey eyes than in young mouse eyes. Both monkey and mouse eyes contain a well-defined Schlemm's canal. Although monkey eyes are considered morphologically similar to human eyes compared with mouse eyes, the uveoscleral outflow estimation may be more similar between monkey and human eyes. However, a washout effect was observed in monkey eyes[37] but not in the mouse[38] and human eyes.[39,40] Therefore, studies of the outflow systems in both species are valuable for future applications in human eyes.

Apart from the morphological differences, age is another potential reason for the different rates of uveoscleral outflow relative to the total outflow between mice (C57BL/6J, 2 months old) in our previous study[20] and monkeys (cynomolgus monkey, 20 years old) in the current study. A study for the same strain of mice has shown that as the age increased from 2.5 to 4.5 months to 10 to 12 months, the uveoscleral outflow reduced by 87%.[41] A similar reduction in uveoscleral outflow with age has been observed in humans, where the outflow decreases by about 30% as individuals age from 20 to 30 to 60 years old.[42] A study in young adult cynomolgus monkeys showed the uveoscleral outflow accounts for about 55% of the total outflow.[43] This suggests that the lower uveoscleral outflow relative to total outflow in the current study may be due to older age. However, because the measurement methods differ, the exact changes in uveoscleral outflow, the association with trabecular outflow, and related morphological differences with age in monkey eyes remain unclear. Furthermore, whereas the risk of developing open-angle glaucoma increases with age,[44] the correlation between the reduction in uveoscleral outflow and this increased risk remains unknown.

In conclusion, this study demonstrates a segmental flow pattern in both trabecular and uveoscleral outflow in monkey eyes, which are uncorrelated under normal conditions. Additionally, the uveoscleral outflow is positively correlated with the thickness of the ciliary stroma. This study provides a baseline of tracer intensity circumferentially around healthy monkey eyes in both outflow pathways and their relationship. In the future, we will further investigate the alternation of uveoscleral outflow when trabecular outflow is damaged to better understand the role of both outflow pathways in IOP regulation. Previous studies have demonstrated that the location of trabecular bypass surgery would affect the increase of outflow facility.[13] Because uveoscleral outflow is also segmental, this suggests the importance of investigating the optimal placement of drainage devices and drug administration targeting the uveoscleral outflow, for which more studies are required. Investigating the uveoscleral outflow pathways in greater detail could enhance our understanding of the IOP regulation mechanism and optimize the treatment approaches for more effective management of patients with glaucoma.

Acknowledgments

Supported by the BrightFocus Foundation Grant G2022013S, The Rifkin Family Glaucoma Research Fund, and Massachusetts Lion Research Fund.

Disclosure: **H.-L. Li**, None; **S. Yu**, None; **S. Fan**, None; **C.B. Toris**, None; **H. Gong**, None

References

1. Tripathi RC. Uveoscleral drainage of aqueous humour. *Exp Eye Res*. 1977;25(Suppl):305–308.
2. Goel M, Picciani RG, Lee RK, Bhattacharya SK. Aqueous humor dynamics: a review. *Open Ophthalmol J*. 2010;4:52–59.
3. Toris CB, Gagrani M, Ghate D. Current methods and new approaches to assess aqueous humor dynamics. *Expert Rev Ophthalmo*. 2021;16(3):139–160.
4. Freddo TF, Civan M, Gong H. Aqueous humor and the dynamics of its flow: mechanisms and routes of aqueous humor drainage. In: Albert DM, Miller JW, Azar DT, Young LH, eds. *Albert and Jakobiec's Principles and Practice of Ophthalmology*. Cham, Switzerland: Springer International Publishing; 2022:1989–2033.
5. Bill A. The routes for bulk drainage of aqueous humour in rabbits with and without cyclodialysis. *Doc Ophthalmol*. 1966;20:157–169.
6. Pederson JE, Gaasterland DE, MacLellan HM. Uveoscleral aqueous outflow in the rhesus monkey: importance of uveal reabsorption. *Invest Ophthalmol Vis Sci*. 1977;16(11):1008–1007.
7. Bill A. Basic physiology of the drainage of aqueous humor. *Exp Eye Res*. 1977;25 Suppl:291–304.
8. Bill A, Phillips CI. Uveoscleral drainage of aqueous humour in human eyes. *Exp Eye Res*. 1971;12(3):275–281.

9. Rowson AC, Hogarty DT, Maher D, Liu L. Minimally invasive glaucoma surgery: safety of individual devices. *J Clin Med*. 2022;11(22):6833.
10. Cvenkel B, Kolko M. Current medical therapy and future trends in the management of glaucoma treatment. *J Ophthalmol*. 2020;2020:6138132.
11. Babighian S, Caretti L, Tavolato M, Cian R, Galan A. Excimer laser trabeculotomy vs 180 degrees selective laser trabeculoplasty in primary open-angle glaucoma. A 2-year randomized, controlled trial. *Eye (Lond)*. 2010;24(4):632–638.
12. Wilmsmeyer S, Philippin H, Funk J. Excimer laser trabeculotomy: a new, minimally invasive procedure for patients with glaucoma. *Graefes Arch Clin Exp Ophthalmol*. 2006;244(6):670–676.
13. Strohmaier CA, Wanderer D, Zhang X, et al. Greater outflow facility increase after targeted trabecular bypass in angiographically determined low-flow regions. *Ophthalmol Glaucoma*. 2023;6:570–579.
14. Paula JS, Senger C, Moraes CG. Comparison of the short-term results of nasal and temporal 180 degrees selective laser trabeculoplasties for open-angle glaucoma. *Arq Bras Oftalmol*. 2023;86(3):217–222.
15. Collaborative Normal-Tension Glaucoma Study Group. The effectiveness of intraocular pressure reduction in the treatment of normal-tension glaucoma. *Am J Ophthalmol*. 1998;126(4):498–505.
16. Toris CB, Camras CB. Aqueous Humor Dynamics II Clinical Studies. In: Civan MM, ed. *The eye's aqueous humor: from secretion to glaucoma*. San Diego, CA: Academic Press; 1998.
17. The AGIS Investigators. The Advanced Glaucoma Intervention Study (AGIS): 7. The relationship between control of intraocular pressure and visual field deterioration. *Am J Ophthalmol*. 2000;130(4):429–440.
18. Reina-Torres E, Baptiste TMG, Overby DR. Segmental outflow dynamics in the trabecular meshwork of living mice. *Exp Eye Res*. 2022;225:109285.
19. Swaminathan SS, Oh DJ, Kang MH, et al. Secreted protein acidic and rich in cysteine (SPARC)-null mice exhibit more uniform outflow. *Invest Ophthalmol Vis Sci*. 2013;54(3):2035–2047.
20. Li HL, Ren R, Gong H. Segmental unconventional outflow in mouse eyes. *Invest Ophthalmol Vis Sci*. 2023;64(15):26.
21. Li G, Mukherjee D, Navarro I, et al. Visualization of conventional outflow tissue responses to netarsudil in living mouse eyes. *Eur J Pharmacol*. 2016;787:20–31.
22. Strohmaier CA, McDonnell FS, Zhang XW, et al. Differences in outflow facility between angiographically identified high- versus low-flow regions of the conventional outflow pathways in porcine eyes. *Invest Ophthalmol Vis Sci*. 2023;64(3):29.
23. Huang AS, Saraswathy S, Dastiridou A, et al. Aqueous angiography with fluorescein and indocyanine green in bovine eyes. *Transl Vis Sci Technol*. 2016;5(6):5.
24. Huang AS, Li M, Yang D, Wang H, Wang N, Weinreb RN. Aqueous angiography in living nonhuman primates shows segmental, pulsatile, and dynamic angiographic aqueous humor outflow. *Ophthalmology*. 2017;124(6):793–803.
25. Sosnowik S, Swain DL, Fan S, Toris CB, Gong H. Morphological changes to Schlemm's canal and the distal aqueous outflow pathway in monkey eyes with laser-induced ocular hypertension. *Exp Eye Res*. 2022;219:109030.
26. Sosnowik S, Swain DL, Liu N, Fan S, Toris CB, Gong H. Endothelial glycocalyx morphology in different flow regions of the aqueous outflow pathway of normal and laser-induced glaucoma monkey eyes. *Cells*. 2022;11(15):2452.
27. Huang AS, Camp A, Xu BY, Penteado RC, Weinreb RN. Aqueous angiography: aqueous humor outflow imaging in live human subjects. *Ophthalmology*. 2017;124(8):1249–1251.
28. Cha EDK, Xu J, Gong L, Gong H. Variations in active outflow along the trabecular outflow pathway. *Exp Eye Res*. 2016;146:354–360.
29. Chang JY, Folz SJ, Laryea SN, Overby DR. Multi-scale analysis of segmental outflow patterns in human trabecular meshwork with changing intraocular pressure. *J Ocul Pharmacol Ther*. 2014;30(2–3):213–223.
30. Vranka JA, Bradley JM, Yang YF, Keller KE, Acott TS. Mapping molecular differences and extracellular matrix gene expression in segmental outflow pathways of the human ocular trabecular meshwork. *PLoS One*. 2015;10(3):e0122483.
31. Karimi A, Khan S, Razaghi R, et al. Segmental biomechanics of the normal and glaucomatous human aqueous outflow pathway. *Acta Biomater*. 2024;173:148–166.
32. Bill A. The aqueous humor drainage mechanism in the cynomolgus monkey (Macaca irus) with evidence for unconventional routes. *Invest Ophthalmol*. 1965;4(5):911–919.
33. Bill A. Conventional and uveo-scleral drainage of aqueous humour in the cynomolgus monkey (Macaca irus) at normal and high intraocular pressures. *Exp Eye Res*. 1966;5(1):45–54.
34. Johnson M, McLaren JW, Overby DR. Unconventional aqueous humor outflow: a review. *Exp Eye Res*. 2017;158:94–111.
35. Bernd AS, Aihara M, Lindsey JD, Weinreb RN. Influence of molecular weight on intracameral dextran movement to the posterior segment of the mouse eye. *Invest Ophthalmol Vis Sci*. 2004;45(2):480–484.
36. Toris CB, Zhan GL, Wang YL, et al. Aqueous humor dynamics in monkeys with laser-induced glaucoma. *J Ocul Pharmacol Ther*. 2000;16(1):19–27.
37. Lu Z, Zhang Y, Freddo TF, Gong H. Similar hydrodynamic and morphological changes in the aqueous humor outflow pathway after washout and Y27632 treatment in monkey eyes. *Exp Eye Res*. 2011;93(4):397–404.
38. Lei YA, Overby DR, Boussommier-Calleja A, Stamer WD, Ethier CR. Outflow physiology of the mouse eye: pressure dependence and washout. *Invest Ophthalmol Vis Sci*. 2011;52(3):1865–1871.
39. Scott PA, Overby DR, Freddo TF, Gong H. Comparative studies between species that do and do not exhibit the washout effect. *Exp Eye Res*. 2007;84(3):435–443.
40. Erickson-Lamy K, Schroeder AM, Bassett-Chu S, Epstein DL. Absence of time-dependent facility increase ("washout") in the perfused enucleated human eye. *Invest Ophthalmol Vis Sci*. 1990;31(11):2384–2388.
41. Millar JC, Phan TN, Pang IH, Clark AF. Strain and age effects on aqueous humor dynamics in the mouse. *Invest Ophthalmol Vis Sci*. 2015;56(10):5764–5776.
42. Toris CB, Yablonski ME, Wang YL, Camras CB. Aqueous humor dynamics in the aging human eye. *Am J Ophthalmol*. 1999;127(4):407–412.
43. Bill A. Aqueous humor dynamics in monkeys (Macaca irus and Cercopithecus ethiops). *Exp Eye Res*. 1971;11(2):195–206.
44. Rudnicka AR, Mt-Isa S, Owen CG, Cook DG, Ashby D. Variations in primary open-angle glaucoma prevalence by age, gender, and race: a Bayesian meta-analysis. *Invest Ophthalmol Vis Sci*. 2006;47(10):4254–4261.

Investigative Ophthalmology & Visual Science